Tuning a microcavity-coupled terahertz laser

Fabrizio Castellano,[1] Vezio Bianchi,[1] Lianhe Li,[2] Jingxuan Zhu,[2] Alessandro Tredicucci,[3] Edmund H. Linfield,[2] A. Giles Davies,[2] and Miriam S. Vitiello[1,a)]
[1]*NEST, CNR-Istituto Nanoscienze and Scuola Normale Superiore, Piazza San Silvestro 12, 56127 Pisa, Italy*
[2]*School of Electronic and Electrical Engineering, University of Leeds, Leeds LS2 9JT, United Kingdom*
[3]*Dipartimento di Fisica, Università degli Studi di Pisa, Largo Pontecorvo 6, 56127 Pisa, Italy*

(Received 9 October 2015; accepted 5 December 2015; published online 29 December 2015)

Tunable oscillators are a key component of almost all electronic and photonic systems. Yet, a technology capable of operating in the terahertz (THz)-frequency range and fully suitable for widescale implementation is still lacking. This issue is significantly limiting potential THz applications in gas sensing, high-resolution spectroscopy, hyper-spectral imaging, and optical communications. The THz quantum cascade laser is arguably the most promising solution in terms of output power and spectral purity. In order to achieve reliable, repeatable, and broad tunability, here we exploit the strong coupling between two different cavity mode concepts: a distributed feedback one-dimensional photonic resonator (providing gain) and a mechanically actuated wavelength-size microcavity (providing tuning). The result is a continuously tunable, single-mode emitter covering a 162 GHz spectral range, centered on 3.2 THz. Our source has a few tens of MHz resolution, extremely high differential efficiency, and unprecedented compact and simple design architecture. By unveiling the large potential that lies in this technique, our results provide a robust platform for radically different THz systems exploiting broadly tunable semiconductor lasers. [http://dx.doi.org/10.1063/1.4938207]

High-resolution gas sensing and spectroscopy require tunable single-frequency sources that cover a broad spectral range while providing sufficient spectral resolution and sensitivity to address single molecule detection. An ideal emitter ought to be capable of attaining quickly a target frequency, and then be fine-tuned across a band a few 10's of GHz wide.

Tunable semiconductor lasers and, in particular, quantum cascade lasers (QCLs)[1] are ideal devices for such applications, owing to their small size, stability, and their inherently high spectral purity.[2] To address the operating requirements of high-resolution spectroscopy, solutions include arrays of thermally tunable QCLs,[3,4] or external-cavity approaches where the frequency of a single broadband device is set by frequency-selective external feedback.[5] In the THz region of the electromagnetic spectrum, QCLs are the only single-mode source capable of providing mW power levels in the 2–5 THz band. As such, broadband tunable single-frequency THz QCLs would be an important technology for gas sensing and spectroscopy.[6–9]

The introduction of distributed feedback (DFB) gratings into the QCLs is the most common solution to achieve single-frequency operation. However, DFB lasers provide limited tunability of emission frequency, being constrained by the grating period. DFB lasers can be tuned by changing the effective refractive index of the waveguide dielectric through varying the temperature,[10] by accessing the evanescent field through metallic plungers,[11–13] by reversible material condensation,[14] or by electrical modulation.[15] Alternative solutions exploit sampled grating[16,17] or difference frequency generation approaches.[18,19]

To date, the largest continuous tuning in a THz QCL (~300 GHz) was obtained by integrating a micro-electro-mechanical (MEMS) plunger with a first-order DFB QCL, actuated by an external piezoelectric driver.[11] MEMS techniques naturally add a significant degree of complexity to the device, requiring alignment and assembly on the laser chip. Furthermore, the reduced width of the corrugated wire DFB laser conventionally employed in this design, dramatically limits the achievable output power (μW-levels) and, consequently, the achievable spectroscopic sensitivity.

Commonly, DFB THz QCLs exploit a sequence of rectangular apertures (slits) in the top metallization of a single- [Ref. 20] or double-metal plasmon waveguide.[21] By adjusting the period of the grating, vertical[21] and spot-like edge[22] emission or polarization control[23] can be obtained. Non-periodic gratings[24,25] alternatively allow further manipulation of the output beam. In double-metal waveguide DFB lasers, however, optical power extraction is often a critical issue, since the laser tends to operate on electromagnetic modes having high Q-factors and low radiative efficiency. This can be addressed by either lowering the modal gain of the unwanted modes, via graded heterostructure,[26] or dual-slit unit cell design,[27] in which the outcoupling efficiency can be maximized and manipulated by replacing the DFB slits with two small surface apertures separated by a variable metallic gap. The resulting large photon loss rate allows the resonator to be strongly coupled with an external microcavity via optical feedback.[28] If the eigenfrequencies of the microcavity are tuned to overlap the laser resonator modes, anticrossed mixed modes appear and extend both into the laser resonator and the external cavity. When the laser is designed to operate on the mixed modes, its frequency can then be changed via tuning of the microcavity size. The

a)Author to whom correspondence should be addressed. Electronic mail: miriam.vitiello@sns.it

tuning range that is achievable by this approach depends on the size of the anticrossing gap, which, in turn, is controlled by the photon loss rate of the QCL cavity. To date, a 20 GHz tuning range has been achieved from a single-frequency surface emitting QCL, a value comparable with that achieved through temperature tuning.[21] While still employing a piezoelectric actuator in the assembly, this approach does not require fabrication of an external MEMS component integrated onto the laser chip,[12] and so represents a simpler and potentially more robust approach.

Here, we conceive a compact architecture that dramatically improves the tunability range of single-frequency THz QCLs, engineered into a microcavity-coupled geometry. By exploiting a wide gain bandwidth (600 GHz) and thin (6.3 μm) QCL active region, we design a strongly coupled system comprising a DFB photonic resonator which provides gain, selectively, only on its lower band edge mode and a mechanically actuated wavelength-size micro-cavity which provides tuning.

The QCL design used in our devices is a slightly modified version of the resonant-phonon three quantum-wells structure that has provided the record highest operating temperature to date.[29] Devices were fabricated in a Au/Au double-metal waveguide configuration. After selective removal of the host GaAs substrate and the $Al_{0.5}Ga_{0.5}As$ etch-stop layer by etching, the exposed 10 μm thick active region was then further thinned via wet etching to define three chips having active region thicknesses of 9.8 μm (sample A), 8.0 μm (sample B), and 6.3 μm (sample C). In the case of sample A, the 200-nm-thick top contact layer was the only layer removed. In samples B and C, inhomogeneities due to the wet etching resulted in a thickness variation of ~300 nm across the chip surface. The designed feedback gratings had a dual-slit cell repeated with periodicity $\Lambda = 27.4\,\mu$m. The slits in the periodic cell were 3–4 μm wide and separated by a distance d, so that $d/\Lambda = 0.4$. An absorbing Cr (7 nm) edge was defined around the 1.5 mm long and 140 μm wide grating section, to provide absorbing boundary conditions to the resonator and suppress Fabry-Pérot modes. The lasers chips were symmetrically wire bonded at the edges of the grating (Fig. 1(a)) whilst avoiding any perturbative effects in the far-field.

The external cavity tuning experiments were performed in a helium-flow cryostat coupled to a Fourier-transform infrared spectrometer (FTIR) equipped with a helium-cooled silicon bolometer. The external cavity arrangement comprises a movable aluminum mirror held parallel to the QCL grating plane at a distance L controllable over a 2.5 mm range by an inertial piezoelectric actuator with nanometer accuracy (Fig. 1(b)). Standing waves between the movable mirror and the metallic surface of the laser chip constitute the modes of the external cavity, coupled to the QCL through the second-order grating. In this geometry, the external cavity also operates as a parallel plate waveguide that guides radiation in the x-y plane. The TE modes of the cavity correspond to the ones coupled with the QCL modes through the DFB grating, while the TM modes of the waveguide provide propagation in the x-y plane. Although in an ideal, perfectly vertically emitting system, light would be trapped between the QCL and the top mirror, bouncing back and forth in the z direction, in the real system a fraction of the power is coupled laterally (along the x-axis) into the TM modes of the waveguide via scattering, due to the finite broadening of the DFB emission lobe.

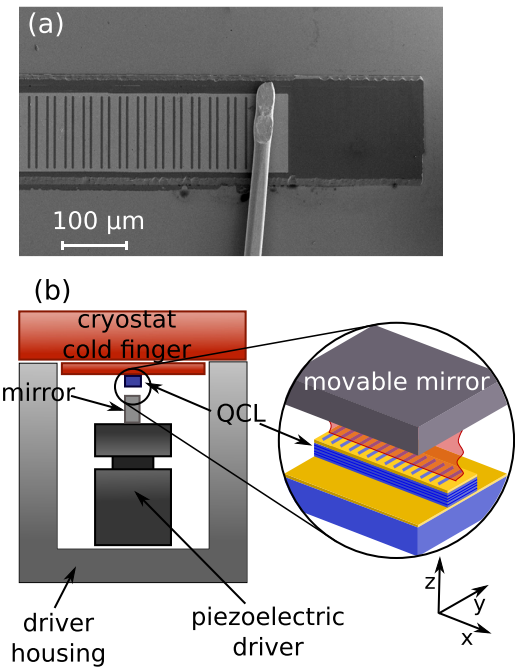

FIG. 1. (a) Scanning electron microscope image of a dual-slit DFB QCL. The absorbing boundary is visible around the grating. (b) Schematic diagram of the external cavity arrangement. The movable mirror was milled from an aluminum block and was then laid on top of the piezoelectric actuator.

When the FTIR spectrometer is scanning the laser emission frequency, we can simultaneously probe the power emitted laterally with a pyroelectric detector. Although, in this latter case, the employed experimental configuration did not allow us to fully optimize the collection efficiency and therefore to carefully quantify the emitted power, we were able to collect more than 25% of the vertically emitted radiation of the freestanding laser.

Two-dimensional finite element calculations were performed to determine the eigenfrequencies of the laser cavity and the coupled laser/microcavity systems. Figures 2(a)–2(c) show the results for samples A, B, and C, respectively, as a function of distance L between the mirror and the QCL grating plane. The mode structure of the coupled system results from the interaction between the two cavities.[28] When the two resonators are coupled, a typical anticrossing curve appears, which describes the eigenfrequencies of the mixed modes of the coupled system, that in turn are the transverse modes of the whole microcavity/wire laser waveguide (blue line in Figs. 2(a)–2(c)). The black dashed lines mark the lower and upper edges of the photonic band gap of the stand-alone DFB QCL, whilst the red lines show the QCL/microcavity photon exchange rates. As the mirror moves, the electromagnetic mode on which the laser operates periodically varies between matching a mode fully localized in the QCL resonator, which has minimal photon loss rate, and a delocalized mode that extends into the external cavity and has maximal photon loss rate. This results in a sequence of tuning regions with periodicity equal to half the free space wavelength of the emitted radiation. Within each tuning

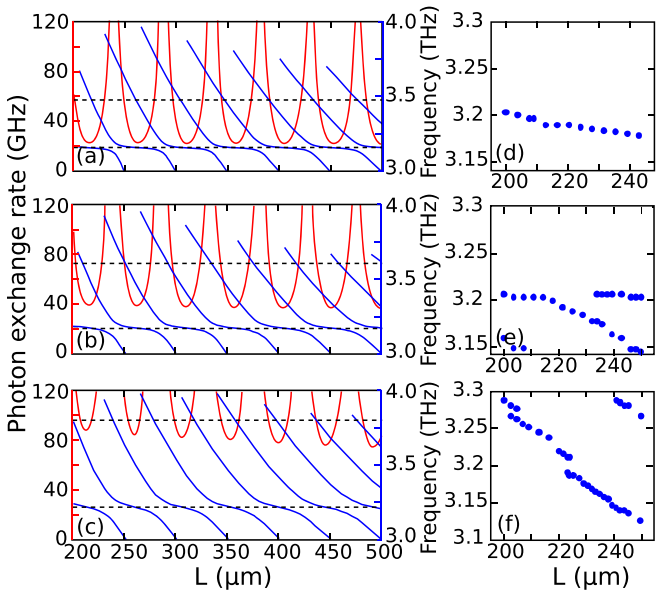

FIG. 2. (a)–(c) Simulated eigenfrequencies of the standalone DFB QCL (dashed black lines) and coupled-cavity system (solid blue lines) and simulated photon loss rates (solid red lines) for samples A (a), B (b), and C (c) as a function of mirror distance L from the QCL surface. (d)–(f) Emission frequencies of samples A (d), B (e), and C (f), plotted as a function of L.

region, the laser frequency follows the anti-crossing curve. As the thickness of the laser resonator becomes smaller, the out-coupling efficiency of the grating increases because the surface fields at the grating apertures intensify owing to the decrease of the modal volume. This effect leads to a faster energy exchange between the two cavities (red lines in Figs. 2(a)–2(c)), which results in the evident increase of the anti-crossing gap, between the lower band-edge mode and the micro-cavity modes (Figs. 2(a)–(c)). It is worth mentioning that the upper band-edge mode does not show anticrossing with the microcavity modes, because in the case of an infinitely periodic structure, this mode is not radiative and consequently cannot couple to the external cavity. Furthermore, being not radiative, it has a quality factor higher than any other mode, which, if matching the QCL bandwidth, could in principle induce the QCL to operate at its frequency.

The calculated photonic lower/upper band edges are 3.16/3.48 THz for sample A (320 GHz bandgap), 3.17/3.61 THz for sample B (440 GHz bandgap) and 3.22/3.81 THz for sample C (590 GHz bandgap). A common feature is that there is a blue shift of the upper band edge with decreasing ridge thickness, which, in all cases, has been designed to lie outside the QCL gain bandwidth. Very different from previous approaches,[28] the rationale is indeed to induce lasing on the radiative lower band-edge mode only. The QCL thickness dependency of its photon exchange rate (minima of the red curves shown in Figs. 2(a)–2(c)) provides a qualitative indication of the corresponding trend in the expected tuning range. Photon exchange rates of 21–22 GHz, 38–40 GHz, and 80–90 GHz were calculated for samples A, B, and C, respectively, when $L = 200$–500 μm. We conclude that thinner cavities lead to increased photon exchange rates and then larger tuning ranges.

A single period of the experimental tuning curve for each sample is plotted in Figs. 2(d)–2(f). We found that sample A shows a maximum tuning of 25 GHz, consistent with previous reports,[28] whilst samples B and C provide remarkably wider tunabilities of 56 GHz and 162 GHz, respectively, in qualitative agreement with the simulations trends shown in Figs. 2(b)–2(c). A significantly larger spectral coverage could be achieved if multiple tuning regions are considered.

Figure 3(a) shows the emission spectra of sample C for different relative mirror positions. In the 430–493 μm range, the QCL frequency varies between 3.190 THz and 3.270 THz, providing 80 GHz mode-hop free tuning. Remarkably, in the 200–250 μm range, the QCL frequency shifts between 3.126 THz and 3.288 THz, i.e., over 162 GHz. This difference is in qualitative agreement with the simulations (Fig. 2(c)), which predict larger photon exchange rates/tuning ranges, at lower mirror distances. The 162 GHz tuning range is interrupted by a few mode hops (attributed to accidental temperature instability (~5 K increase) in the cryostat) and occasional peak-splitting, although the combined frequency coverage provided by all three spans reported in Fig. 3(a) is continuous. Every frequency can thus be achieved in single-mode operation through appropriate adjustment of the mirror position. The observed double-peak emission in the lower mirror distance range can be attributed to the mode competition over the short pulse operation. However, the device is single-mode emitting over a very large mirror position range with a side-mode suppression ratio >20 dB, limit set by the noise floor of the FTIR in rapid-scan acquisition mode. Figure 3(a) also shows that there is an overlap between the tuning regions, meaning that at selected mirror positions the QCL provides dual-frequency emission (e.g., the spectrum at a 50 μm mirror distance). By removing such dual-frequency windows, single frequency tuning of 144 GHz can be achieved. The reached impressive tuning range is the result of the improved photon exchange rate, achieved via the combined action of the wide active region bandwidth, reduced thickness, and lower-band-edge

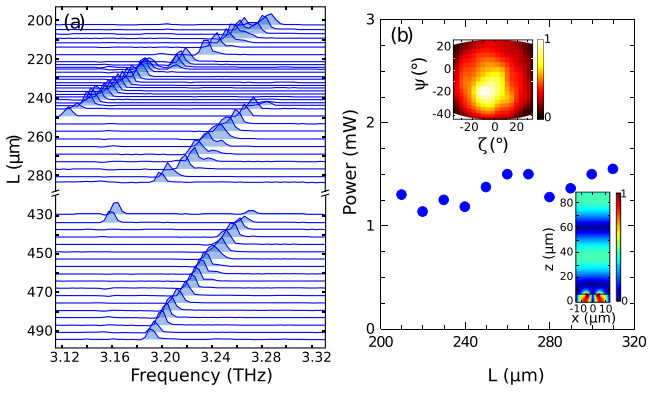

FIG. 3. (a) Emission spectra of sample C acquired at 20 K, in rapid-scan mode with a resolution of 0.25 cm^{-1}, whilst moving the external cavity mirror over a large distance. Spectra have been normalized and offset so that the baseline in each case corresponds to the mirror position shown on the vertical axis; (b) emitted optical power of sample C collected a function of the mirror position (L) while scanning the pyroelectric detector in the (y-z) plane of Fig. 1. Upper-left inset: far-field emission pattern of sample C measured at 900 A/cm^2 as a function of elevation (ζ) and azimuth (ψ) angles with respect to the (y-z) plane. Lower-right inset: simulated electric field norm of the upper mode of the coupled cavity at the anticrossing point, with the mirror position set to 250 μm.

DFB resonator. It is worth mentioning that no lasing has been observed at frequencies around the predicted upper band edge mode (3.8 THz) for all mirror positions.

The frequency resolution of our tunable QCL is set by the accuracy of the mirror positioning. The periodicity of the tuning curve is 50 μm (tuning rate of 3.2 GHz/μm in one period), corresponding on average to ~300 steps of the piezoelectric actuator driven at 20 V. Since we measured a different frequency shift in individual periods of the tuning curve (Fig. 3(a)), the attainable resolution varies accordingly, with a minimum extrapolated value of 270 MHz, corresponding to the movable mirror range 430–493 μm range (Fig. 3(a)). This value, limited by the stepping of the piezoelectric actuator, is much smaller than the achievable resolution of our FTIR spectrometer, and so cannot be measured directly. By reducing the drive voltage of the piezoelectric actuator, the resolution can be reduced by a further one order of magnitude (30 MHz). The optical power emitted laterally (x-axis) is almost independent from the mirror position (Fig. 3(b)) (and therefore from the frequency) and 25% of the vertically emitted power. The lower-right inset of Fig. 3(b) shows the simulated electric field norm of the upper mode of the coupled cavity at the anti-crossing point. In this condition, the mode is a superposition of a TE cavity mode and the lower bandgap mode of the DFB. In the QCL system, a fraction of the light is indeed expected to be scattered sideways due to the finite size of the QCL resonator. The above claim is supported by the lack of dependence of the far-field shape (upper-left inset Fig. 3(b)) on the mirror position.

Figure 4 shows the vertically emitted light-current-voltage (LIV) curves for samples A, B, and C, measured in pulsed mode (200 ns pulse width, 25 kHz repetition rate) and in the surface normal direction, for a double-metal QCL with an identical active region (but no patterning) as a reference.

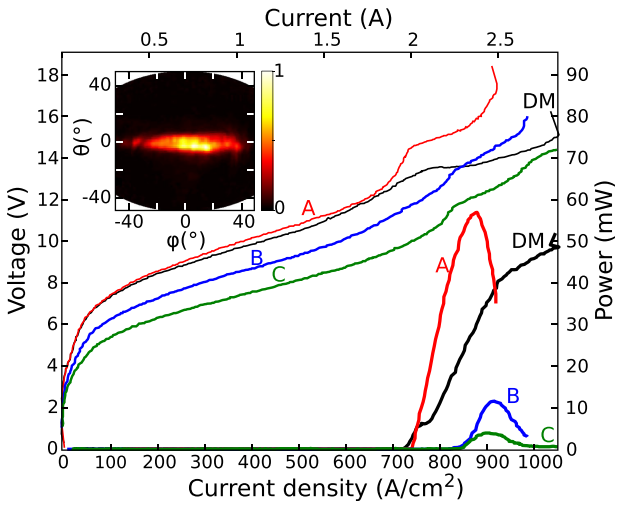

FIG. 4. Light-current-voltage characteristics of samples A, B, and C measured at 20 K in the surface normal direction, compared with a standard-double metal QCL (labeled as DM) processed from the same epitaxial wafer. Absolute emitted powers were obtained by integrating over the far-field emission patterns. Inset: far-field emission pattern of sample A measured by employing a x–y translation stage, driven by stepper motors with a spatial resolution of ~0.2 μm, along the z-axis (no mirror on the top) at 850 A/cm^2 as a function of elevation (θ) and azimuth (φ) angles with respect to the surface normal, demonstrating that the DFB device emits exclusively on the low-frequency DFB mode.

For the reference sample, the total power emitted from the two facets is shown. The threshold current and peak output power (60 mW) of sample A are comparable with those recorded for the reference double-metal sample. However, the DFB QCL shows a remarkably higher slope-efficiency of ~210 mW/A, than that of the reference QCL (100 mW/A), which is a clear indication of the improved extraction efficiency of the DFB laser when operating on its radiative mode. Samples B and C have slope efficiencies of 116 mW/A and 52 mW/A, respectively.

Despite the higher radiative efficiency, samples B and C, having thinner active regions, lase, as expected,[30] at lower voltages, with larger threshold current densities and reduced output powers. The increased threshold current values are a clear signature of the lower modal gain, resulting from the increased optical losses. No variation of the threshold current as a function of the mirror position was observed, indicating that the radiation losses are not playing any role on the achievable lasing threshold. Although the simulations of Figs. 2(a)–2(c) predict an increase in radiative losses as the active region becomes thinner, an important role is played by the ohmic losses, which increase as the waveguide thickness decreases[30] and by inhomogeneities in the sample thickness induced by the wet etching process.

The single lobe emission pattern shown in the inset of Fig. 4 for sample A, which is common to all samples, unambiguously proves that the QCLs are operating on the radiative mode located at the lower edge of the photonic bandgap, as designed. The wide photonic bandgap then pushes the upper band-edge mode (high-Q, non-radiative) outside of the active region gain bandwidth, as expected.

The achieved tunability is a record for any single-mode surface-emitting THz QCL, and the combined power and slope-efficiency performance provides a valuable alternative to QCL-MEMS configurations for practical applications. The concept can be further extended to target specific application requirements. For example, continuous-wave (CW) operation can be achieved by employing a different active region design with lower threshold current densities,[26] where the thinner structures with low applied voltages can easily induce CW-operation even in devices with a large resonator footprint. This is a distinct advantage compared to wire lasers,[11] whose cross-section must be kept comparable to the wavelength in order for the optical mode to leak out laterally, thus limiting the achievable absolute power. Furthermore, refined movable mirror housing architectures, could be implemented; THz reflectors might allow achieving collection efficiencies >50%, with a required accuracy for lateral alignment of the order of the beam waist at the focal point, and can be combined with THz flexible hollow fibers attached to the laser facet. Finally, further improvement of the spectral coverage can be envisaged using a more refined micro-cavity design, for example, by replacing the flat mirror with a geometry that optimizes the optical feedback into the QCL.

This work was partly supported by the Italian Ministry of Education, University, and Research (MIUR) through the program FIRB-Futuro in Ricerca 2010, RBFR10LULP, "Fundamental research on terahertz photonic devices," the

EPSRC (UK), and the ERC programs "TOSCA" and "SoulMan." We also acknowledge the support of the Royal Society and the Wolfson Foundation. The authors acknowledge R. Colombelli for the technical support in the QCL double-waveguide fabrication.

[1]M. S. Vitiello, G. Scalari, B. S. Williams, and P. De Natale, "Quantum cascade lasers: 20 years of challenges," Opt. Express **23**, 5167–5182 (2015).
[2]M. S. Vitiello, L. Consolino, S. Bartalini, A. Taschin, A. Tredicucci, M. Inguscio, and P. De Natale, "Quantum-limited frequency fluctuations in a terahertz laser," Nat. Photonics **6**, 525–528 (2012).
[3]B. G. Lee, M. A. Belkin, C. Pflügl, L. Diehl, H. A. Zhang, R. M. Audet, J. MacArthur, D. P. Bour, S. W. Corzine, G. E. Höfler, and F. Capasso, "DFB quantum cascade laser arrays," IEEE J. Quant. Electron. **45**, 554–565 (2009).
[4]P. Rauter, S. Menzel, A. K. Goyal, C. A. Wang, A. Sanchez, G. Turner, and F. Capasso, "High-power arrays of quantum cascade laser master-oscillator power-amplifiers," Opt. Express **21**, 4518 (2013).
[5]A. Hugi, R. Terazzi, Y. Bonetti, A. Wittmann, M. Fischer, M. Beck, J. Faist, E. Gini, and A. Hugi, "External cavity quantum cascade laser tunable form 7.6 μm to 11.4 μm," Appl. Phys. Lett. **95**, 61103 (2009).
[6]S. Kumar, "Recent progress in terahertz quantum cascade lasers," IEEE J. Sel. Top. Quant. Electron. **17**, 38 (2011).
[7]L. Consolino, A. Campa, M. Ravaro, D. Mazzotti, M. S. Vitiello, S. Bartalini, and P. De Natale, "Saturated absorption in a rotational molecular transition at 2.5 THz using a quantum cascade laser," Appl. Phys. Lett. **106**, 021108 (2015).
[8]S. Borri, P. Patimisco, A. Sampaolo, H. E. Beere, D. A. Ritchie, M. S. Vitiello, G. Scamarcio, V. Spagnolo, and S. Borri, "Terahertz quartz enhanced photo-acoustic sensor," Appl. Phys. Lett. **103**, 021105 (2013).
[9]P. Dean, A. Valavanis, J. Keeley, K. Bertling, Y. L. Lim, R. Alhathlool, A. D. Burnett, L. H. Li, S. P. Khanna, D. Indjin, T. Taimre, A. D. Rakić, E. H. Linfield, and A. G. Davies, J. Phys. D: Appl. Phys. **47**, 374008 (2014).
[10]M. S. Vitiello and A. Tredicucci "Tunable emission in THz quantum cascade lasers," IEEE Trans. Terahertz Sci. Technol. **1**, 76 (2011).
[11]Q. Qin, B. S. Williams, S. Kumar, J. L. Reno, and Q. Hu, "Tuning a terahertz wire laser," Nat. Photonics **3**, 732–737 (2009).
[12]Q. Qin, J. L. Reno, and Q. Hu, "MEMS-based tunable terahertz wire-laser over 330 GHz," Opt. Lett. **36**, 692–694 (2011).
[13]N. Han, A. de Geofroy, D. P. Burghoff, C. W. Chan, A. W. Lee, J. L. Reno, and Q. Hu, "Broadband all-electronically tunable MEMS terahertz quantum cascade lasers," Opt. Lett. **39**, 3480–3483 (2014).
[14]D. Turchinkova, M. I. Amanti, F. Castellano, M. Beck, and J. Faist, "Continuous tuning of terahertz distributed feedback quantum cascade laser by gas condensation and dielectric deposition," Appl. Phys. Lett. **102**, 181113 (2013).
[15]K. Ohtani, M. Beck, and J. Faist, "Electrical laser frequency tuning by three terminal terahertz quantum cascade lasers," Appl. Phys. Lett. **104**, 011107 (2014).
[16]T. S. Mansuripur, S. Menzel, R. Blanchard, L. Diehl, C. Pflügl, Y. Huang, J.-H. Ryou, R. D. Dupuis, M. Loncar, and F. Capasso, "Widely tunable mid-infrared quantum cascade lasers using sampled grating reflectors," Opt. Express **20**, 23339 (2012).
[17]S. Slivken, N. Bandyopadhyay, Y. Bai, Q. Y. Lu, and M. Razeghi, "Extended electrical tuning of quantum cascade lasers with digital concatenated gratings," Appl. Phys. Lett. **103**, 231110 (2013).
[18]Q. Y. Lu, S. Slivken, N. Bandyopadhyay, Y. Bai, and M. Razeghi, "Widely tunable room temperature semiconductor terahertz source," Appl. Phys. Lett. **105**, 201102 (2014).
[19]K. Vijayraghavan, Y. Jiang, M. Jang, A. Jiang, K. Choutagunta, A. Vizbaras, F. Demmerle, G. Boehm, M. C. Amann, and M. A. Belkin, Nat. Commun. **4**, 2021 (2013).
[20]L. Ajili, J. Faist, H. Beere, D. Ritchie, G. Davies, and E. Linfield, "Loss-coupled distributed feedback far-infrared quantum cascade lasers," Electron. Lett. **41**, 419 (2005).
[21]S. Kumar, B. S. Williams, Q. Qin, A. W. M. Lee, Q. Hu, and J. L. Reno, "Surface-emitting distributed feedback terahertz quantum-cascade lasers in metal-metal waveguides," Opt. Express **15**, 113–128 (2007).
[22]M. I. Amanti, G. Scalari, F. Castellano, M. Beck, and J. Faist, "Low divergence terahertz photonic wire laser," Opt. Express **18**, 6390–6395 (2010).
[23]P. Rauter, J. Lin, P. Genevet, S. P. Khanna, M. Lachab, A. Giles Davies, E. H. Linfield, and F. Capasso, "Electrically pumped semiconductor laser with monolithic control of circular polarization," Proc. Natl. Acad. Sci. U. S. A. **111**, E5623 (2014).
[24]M. S. Vitiello, M. Nobile, A. Ronzani, A. Tredicucci, F. Castellano, V. Talora, L. Li, E. H. Linfield, and A. G. Davies, "Photonic quasi-crystal terahertz lasers," Nat. Commun. **5**, 5884 (2014).
[25]F. Castellano, S. Zanotto, L. H. Li, A. Pitanti, A. Tredicucci, E. H. Linfield, A. G. Davies, and M. S. Vitiello, "Distributed feedback terahertz frequency quantum cascade lasers with dual periodicity gratings," Appl. Phys. Lett. **106**, 011103 (2015).
[26]G. Xu, R. Colombelli, S. P. Khanna, A. Belarouci, X. Letartre, L. Li, E. H. Linfield, A. G. Davies, H. E. Beere, and D. A. Ritchie, "Efficient power extraction in surface-emitting semiconductor lasers using graded photonic heterostructures," Nat. Commun. **3**, 952 (2012).
[27]L. Mahler, A. Tredicucci, F. Beltram, C. Walther, J. Faist, H. E. Beere, and D. A. Ritchie, "High-power surface emission from terahertz distributed feedback lasers with a dual-slit unit cell," Appl. Phys. Lett. **96**, 191109 (2010).
[28]L. Mahler, A. Tredicucci, F. Beltram, H. E. Beere, and D. A. Ritchie, "Tuning a distributed feedback laser with a coupled microcavity," Opt. Express **18**, 19185–19191 (2010).
[29]S. Fathololoumi, E. Dupont, C. W. I. Chan, Z. R. Wasilewski, S. R. Laframboise, D. Ban, A. Matyas, C. Jirauschek, Q. Hu, and H. C. Liu, "Terahertz quantum cascade lasers operating up to 200 K with optimized oscillator strength and improved injection tunneling," Opt. Express **20**, 3866 (2012).
[30]Y. Chassagneux, J. Palomo, R. Colombelli, S. Barbieri, S. Dhillon, C. Sirtori, H. Beere, J. Alton, and D. Ritchie, "Low threshold THz QC lasers with thin core regions," Electron. Lett. **43**, 285–286 (2007).